BIOCHEMISTRY
including biophysical chemistry & molecular biology
Article

Biochemistry **2009,** *48,* 11243–11251 11243
DOI: 10.1021/bi901501a

Identification of the Rate-Determining Step of tRNA-Guanine Transglycosylase from *Escherichia coli*[†]

George A. Garcia,* Stephanie M. Chervin, and Jeffrey D. Kittendorf

Department of Medicinal Chemistry, College of Pharmacy, University of Michigan, Ann Arbor, Michigan 48109-1065

Received August 27, 2009; Revised Manuscript Received October 29, 2009

ABSTRACT: The modified RNA base queuine [7-(4,5-*cis*-dihydroxy-1-cyclopenten-3-ylaminomethyl)-7-deazaguanine] is present in tRNA because of a unique base-exchange process catalyzed by tRNA-guanine transglycosylase (TGT). Previous studies have suggested the intermediacy of a covalent TGT−RNA complex. To exist on the reaction pathway, this covalent complex must be both chemically and kinetically competent. Chemical competence has been demonstrated by the crystal structure studies of Xie et al. [(2003) *Nat. Struct. Biol. 10*, 781−788]; however, evidence of kinetic competence had not yet been established. The studies reported here unequivocally demonstrate that the TGT−RNA covalent complex is kinetically capable of occurring on the TGT reaction pathway. These studies further suggest that dissociation of product RNA from the enzyme is overall rate-limiting in the steady state. Interestingly, studies comparing RNA with a 2′-deoxyriboside at the site of modification suggest a role for the 2′-hydroxyl group in stabilizing the growing negative charge on the nucleophilic aspartate (264) as the glycosidic bond to the aspartate is broken during the breakdown of the covalent complex.

More than 100 chemically distinct modified bases are known to occur in RNA, the majority of which occur in tRNA (*1*). Of these, queuine (Q)[1] stands out for several reasons. Structurally, queuine is the only modified base that is not a purine or pyrimidine analogue. Instead, queuine features a pyrrolo-pyrimidine heterocyclic scaffold that is further elaborated through exocyclic chemical modifications. Perhaps most interestingly, the mechanism of incorporation of queuine into tRNA is unique. The queuine base is post-transcriptionally introduced into tRNA via a transglycosylation reaction that is catalyzed by tRNA-guanine transglycosylase (TGT) (Figure 1). Among the known modified bases, only pseudouridine is installed in an analogous manner whereby pseudouridine synthase breaks and re-forms the glycosidic bond to the uracil (*2*).

As with pseudouridine synthase, the chemical mechanism of the TGT reaction has been studied for some time. Two distinct mechanisms have been proposed and subsequently investigated for the TGT-catalyzed base-exchange reaction. It was first envisaged that a dissociative mechanism, involving the intermediacy of an oxocarbonium ion, could drive the cleavage of the glycosidic bond leading to the incorporation of the modified base. Alternatively, and equally plausible, the TGT reaction may proceed through a covalent TGT−RNA intermediate (*3*) in an associative mechanism similar to that of retaining glycosyl hydrolases (*4*) (Figure 2A). In fact, biochemical studies from our laboratory have implicated the associative mechanism and the involvement of two active site aspartate residues in the reaction (*5*, *6*). Consistent with the associative mechanism, we have previously shown that the *Escherichia coli* TGT follows ping-pong kinetics (*7*), with RNA binding first, followed by guanine release, binding of $preQ_1$, and finally release of product RNA (Figure 2B). More recently, the X-ray crystal structure of a TGT−RNA complex (Figure 3) has revealed that aspartate 264 can form a covalent bond with the ribose of the RNA. Furthermore, upon addition of $preQ_1$, the covalent complex converted to free TGT and product RNA.

While compelling, these studies are not sufficient to definitively prove the intermediacy of the covalent complex. For example, it is possible that during the crystallization process, aspartate 264 could have trapped a carbonium ion intermediate. To be considered an intermediate in an enzymic reaction, the covalent complex must be both chemically competent (i.e., it must form from substrates and react to form the correct products) and kinetically competent (i.e., the intermediate must form and break down at a rate equal to or greater than k_{cat}). To provide clear evidence for the associative mechanism, we have conducted studies to determine the kinetic competence of the covalent complex. The results of these experiments indicate that the TGT−RNA covalent complex is kinetically competent and therefore can exist on the TGT reaction pathway. Through this analysis, we have also identified the rate-limiting step in the TGT reaction and find evidence suggesting a role for the 2′-hydroxyl group of the ribose in the TGT reaction.

EXPERIMENTAL PROCEDURES

Reagents. Unless otherwise specified, reagents were purchased from Sigma or Aldrich. Isopropyl β-D-thiogalactopyranoside (IPTG) and dithiothreitol (DTT) were from Invitrogen.

[†]This work was supported in part by the National Institutes of Health (Grant GM065489 to G.A.G. and Grant GM07767 to J.D.K., trainee) and the University of Michigan, College of Pharmacy, Vahlteich, and UpJohn Research Funds.

*To whom correspondence should be addressed: Department of Medicinal Chemistry, College of Pharmacy, University of Michigan, Ann Arbor, MI 48109-1065. Phone: (734) 764-2202. Fax: (734) 647-8430. E-mail: gagarcia@umich.edu.

[1]Abbreviations: DTT, dithiothreitol; ECYMH, hairpin RNA corresponding to the $tRNA^{tyr}$ anticodon stem−loop motif; HEPES, hydroxyethylpiperazineethane sulfonate; PAGE, polyacrylamide gel electrophoresis; PMSF, phenylmethanesulfonyl fluoride; Q, queuine; RRU, relative response units; SDS, sodium dodecyl sulfate; SPR, surface plasmon resonance; TCA, trichloroacetic acid; TGT, tRNA-guanine transglycosylase; Tris·HCl, tris(hydroxymethyl)aminomethane hydrochloride.

Published on Web 10/29/2009

Ampicillin, kanamycin, and chloramphenicol were from Boehringer Mannheim. HEPES (1 M solution, pH 7.3), precast PhastGels, and SDS buffer strips were from Pharmacia. Tris·HCl buffer was from Research Organics. His·Bind resin was from Novagen. Bactotryptone and yeast extract were from Difco. Bradford reagent and BSA standards were from Bio-Rad. [8-^{14}C]Guanine (56 mCi/mmol) was from Moravek. Reagents for RNA chemical synthesis were from Applied Biosystems, with the exception of the RNA and DNA (dG) phosphoramidite monomers and the CPG columns, which were from Glen Research. *E. coli* tRNA-guanine transglycosylase (TGT) and the D264N mutant were prepared as previously described (*5*, *6*).

Chemical Synthesis of Hairpin RNAs. The hairpin RNAs ECYMH (5′-GGGAGCAGACUGUAAAUCUGCUCCC-3′) and (dG)$_{34}$ECYMH (5′-GGGAGCAGACUdGUAAAUCUGCUCCC-3′) were synthesized by automated chemical synthesis performed on an Expedite nucleic acid synthesis system (model 8909, PerSeptive Biosystems) and purified as previously described (*5*, *6*) or were purchased from Dharmacon. Biotinylated hairpin RNAs [bio-ECYMH and bio-(dG)$_{34}$ECYMH] were purchased from Dharmacon.

Preparation of PreQ$_1$-Containing RNA Minihelices. In a reaction volume of 200 μL, the substrate RNA [ECYMH, (dG)$_{34}$ECYMH, bio-ECYMH, or bio-(dG)$_{34}$ECYMH, 80 μM] was incubated with preQ$_1$ (200 μM) and TGT (1.4 μM) in bicine reaction buffer (bicine at 50 mM and pH 8.1) at 37 °C for 18 h. The reaction was quenched by precipitation upon addition of 10 M ammonium acetate (low sodium) to a final concentration of 1 M and 750 μL of ethanol (reagent grade) and the mixture cooled at −20 °C for 8 h. The precipitated RNA was recovered by centrifugation and purified twice more by ethanol precipitation. The resulting RNA pellet was resuspended in ultrapure water to a final concentration of 50 μM and stored at −20 °C. The guanine/preQ$_1$ substitution was confirmed by MALDI mass spectrometry

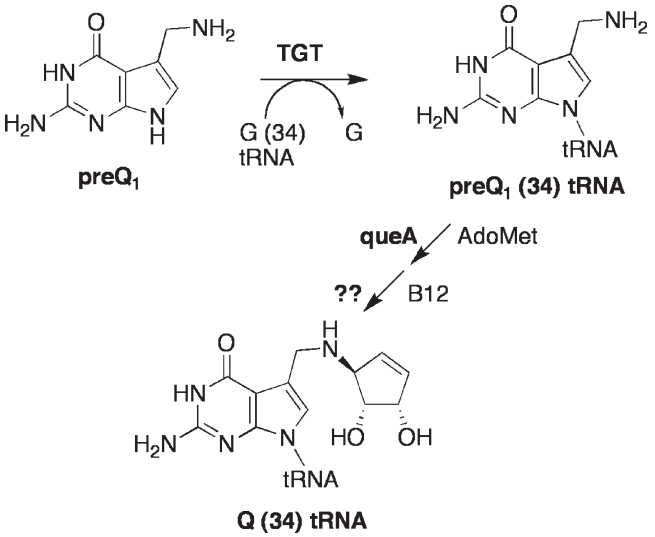

FIGURE 1: Eubacterial tRNA-guanine transglycosylase (TGT) pathway.

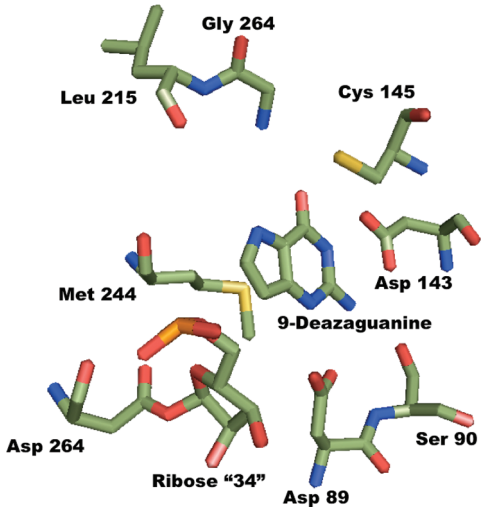

FIGURE 3: X-ray crystal structure of the *Zymomonas mobilis* TGT−RNA covalent complex trapped with 9-deazaguanine. Generated from Protein Data Bank entries 1Q2R and 1Q2S (*12*).

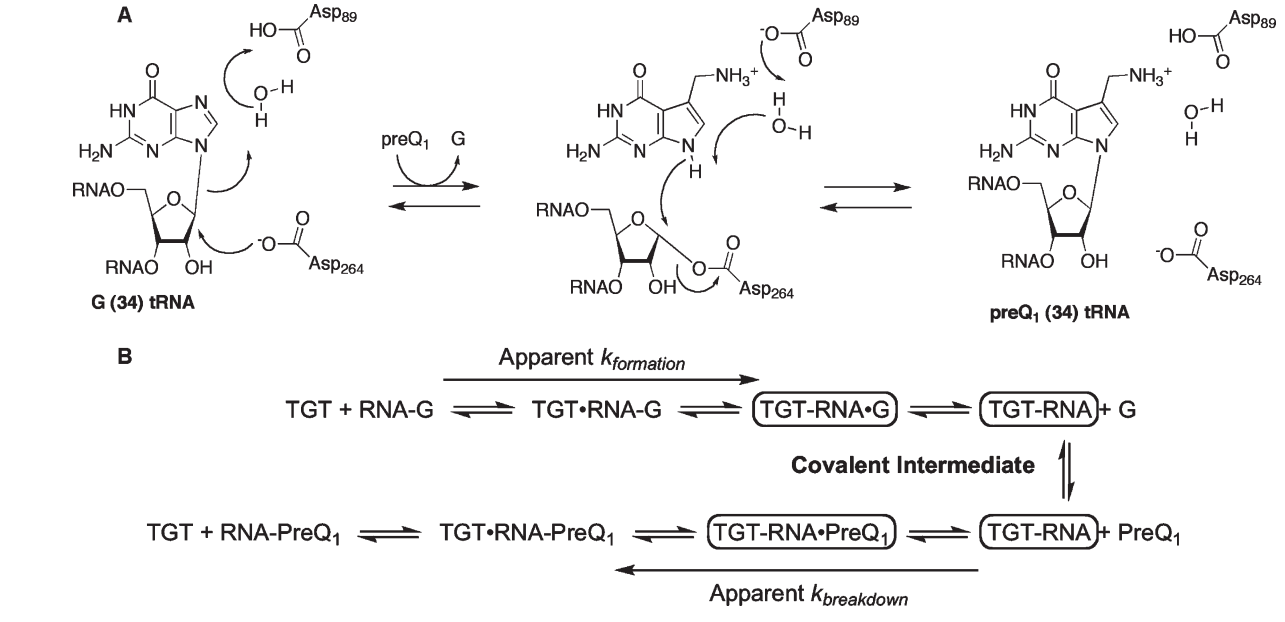

FIGURE 2: *E. coli* TGT chemical and kinetic mechanisms. (A) Chemical mechanism involving nucleophilic catalysis by aspartate 264. (B) Ping-pong kinetic mechanism. Intermediates containing the covalent TGT−RNA complex are circled.

by confirming the 28 mass unit differential between the guanine-containing and $preQ_1$-substituted RNA (see the Supporting Information).

Steady-State Kinetics for ECYMH and $(dG)_{34}$ECYMH. Substrate RNA at concentrations ranging from 0.1 to 30.0 μM was incubated with [^{3}H]$preQ_1$ (20 μM) in bicine assay buffer [bicine (50 mM, pH 8.1), $MgCl_2$ (20 mM), and DTT (5 mM)] at 37 °C. The reaction was initiated by the addition of *E. coli* TGT to a final enzyme concentration of 100 nM. At specific intervals (1, 4, 8, 12, and 20 min), an aliquot (70 μL) of the reaction mixture was quenched with 10 μL of NaOAc (3 M, pH 5.5) followed immediately by precipitation in 900 μL of ethanol. The quenched samples were cooled to −20 °C for 2 h. The precipitated RNA substrate was captured by filtration through a Whatman GF/C filter. The filter was immersed in BioSafeII LSC cocktail, and the amount of tritium incorporation was determined by liquid scintillation counting. Initial velocities (v_i) were determined from plots of picomoles of [^{3}H]$preQ_1$ incorporated versus time. k_{cat} and K_M values were determined from nonlinear fits of v_i versus RNA substrate concentration to eq 1 (Michaelis−Menten).

$$v_i = \frac{k_{cat}[TGT][RNA]}{K_M + [RNA]} \quad (1)$$

Rate of Covalent Intermediate Formation. The apparent rates of formation of the TGT−RNA covalent intermediates for ECYMH and $(dG)_{34}$ECYMH were assayed as previously described (*8*) with modifications. A KinTek RQF-3 rapid chemical quench-flow apparatus was charged with drive buffer (bicine at 50 mM and pH 8.1) and SDS quench buffer [Tris·HCl (60 mM, pH 7.0) and 2% SDS] and equilibrated to 37 °C. Sample port A was loaded with a solution of enzyme, TGT (15 μM), in bicine assay buffer, and sample port B was loaded with a solution of RNA substrate (30 μM) also in bicine assay buffer. Aliquots (15 μL) of each reagent were incubated in the mixing chamber for various periods of time (0.5−120.0 s) and the reactions quenched automatically with SDS buffer (90 μL). The mixtures were incubated for an additional 1 h at room temperature prior to SDS−PAGE band-shift analysis. Aliquots (4 μL) of each reaction were loaded onto a gradient 8 to 25% polyacrylamide gel (Pharmacia Phast System, now GE Healthcare) and run under denaturing conditions following the vendor protocols. The gel was removed from the plastic backing and stained with Sypro-Red. The bands were visualized by green laser excitation (532 nm) and fluorescence detection using a Typhoon 9200 gel imaging system (Molecular Dynamics). The percent covalent intermediate was calculated from the band volumes, which were quantified with ImageQuant (Molecular Dynamics) as described previously (*8*). Assays were conducted in triplicate, and the apparent first-order rate constants ($k_{formation}$) for formation of the TGT−RNA intermediates were determined by exponential fits of the data to eq 2:

$$y = M(1 - e^{-k_{formation}t}) \quad (2)$$

where y is the percent covalent complex formed, t is the time in seconds, and M is the maximum percent covalent complex.

Isolation of the TGT−$(dG)_{34}$ECYMH Covalent Intermediate. TGT (50 μM) and $(dG)_{34}$ECYMH (75 μM) were incubated in bicine assay buffer in a total reaction volume of 100 μL for 20 min at 37 °C. The mixture was cooled to 4 °C and diluted with 200 μL of Ni^{2+} column binding buffer [Tris·HCl (20 mM, pH 7.9), NaCl (500 mM), and imidazole (10 mM)]. The covalent intermediate and any unreacted free TGT were isolated from the reaction mixture via Ni^{2+} affinity chromatography, taking advantage of the His-tagged TGT. Ni-NTA resin (50 μL, His·Bind, Novagen) was added to the mixture, and the slurry was applied to a disposable plastic column. The column was washed with 20 mM imidazole in binding buffer to remove unbound RNA. The TGT−$(dG)_{34}$ECYMH intermediate and free TGT were eluted with 250 mM imidazole in binding buffer. The eluted material was exchanged into bicine buffer and analyzed by SDS−PAGE. The isolation of the covalent intermediate was confirmed by MALDI-TOF mass spectrometric analysis. The matrix was 2,4,6-trihydroxyacetophenone (10 mg/mL) and ammonium citrate (5 mg/mL) in a 1:1 acetonitrile/water mixture. The following ions were detected: (m + 1)/1 at 52449 and (m + 1)/2 at 26187.

Rate of Covalent Intermediate Breakdown. The apparent rate of formation of the TGT−$(dG)_{34}$ECYMH intermediate was assayed in a fashion similar to that for the apparent rate of formation of the covalent intermediate. The TGT−$(dG)_{34}$ECYMH and TGT mixture (15 μL, 6 μM) was mixed with a solution of $preQ_1$ (15 μL, 1.2 mM) and quenched in SDS buffer over a time course ranging from 0.01 to >20 s using a KinTek rapid-quench apparatus as described above. The quenched samples were then separated by SDS−PAGE and quantified as described above. Assays were conducted in triplicate, and the apparent first-order rate constant ($k_{breakdown}$) for breakdown of the TGT−$(dG)_{34}$ECYMH intermediate was determined by an exponential fit of the data to eq 3:

$$y = (M_1 - M_2)(e^{-k_{breakdown}t}) + M_2 \quad (3)$$

where y is the percent covalent complex remaining, t is the time in seconds, M_1 is the maximum percent covalent complex, and M_2 is the minimum percent covalent complex.

Association and Dissociation Kinetics via Surface Plasmon Resonance. Surface plasmon resonance studies were conducted on a BIAcore 3000 instrument (GE Healthcare Life Sciences). Strepavidin (SA) sensor chips were purchased from GE Healthcare. Running buffer was the same bicine assay buffer used for the steady-state kinetics with the addition of 0.1% Tween [which had no effect on enzyme activity (data not shown)]. The sensor chip surface was equilibrated with running buffer at a rate of 10 μL/min for 2−4 h. Biotinylated RNA [e.g., bio-$(dG)_{34}$ECYMH] was loaded onto the sensor chip via sequential injections of 5 or 10 μL. Lane 1 of the sensor chip was used as a blank control lane. The biotinylated RNA injections were repeated, as needed, to yield approximate loadings of 800, 1500, and 2500 response units (RU) in lanes 2−4, respectively. The RNAs were stably associated with the sensor chip surface as evidenced by constant RU values for each lane after replicate regeneration injections and throughout the course of each experiment.

Ten different concentrations of TGT (D264N), ranging from 0.05 to 7.5 μM, were passed over the sensor chip at a rate of 10 μL/min and a temperature of 37 °C. Injection volumes varied between 20 and 40 μL to establish equilibrium binding during the association phase. The dissociation phase was monitored for 120−240 s. Regeneration of the sensor chip [e.g., complete dissociation of TGT(D264N)] was achieved by injection of 20−40 μL of 2 or 6 M guanidine hydrochloride in running buffer.

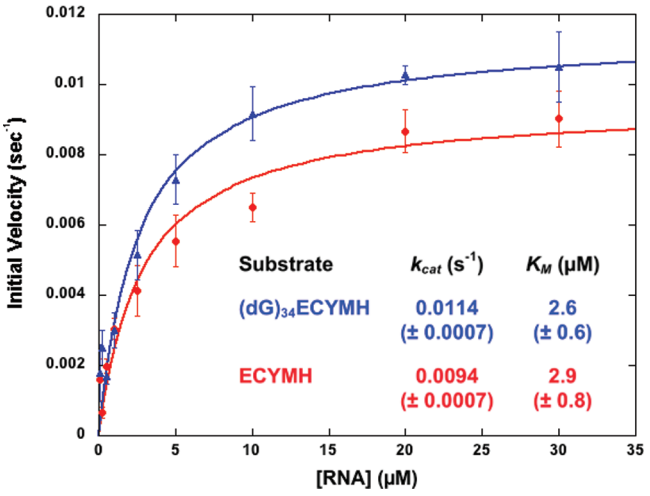

FIGURE 4: Steady-state kinetics of incorporation of preQ$_1$ for ECYMH and (dG$_{34}$)ECYMH. Fits of initial velocity vs RNA concentration to the Michaelis−Menten equation: $v_i = (k_{cat}[TGT])/(K_M + [RNA])$. Error bars are standard deviations of the averages of three independent trials. Kinetic parameters are reported with standard errors in parentheses.

Sensorgram data were analyzed using BIA Evaluation (GE Healthcare Life Sciences). The data best fit to the "two-state (conformational change) model" (eq 4):

$$A + B \underset{k_{off}}{\overset{k_{on}}{\rightleftharpoons}} AB \underset{k_{reverse}}{\overset{k_{forward}}{\rightleftharpoons}} AB* \quad (4)$$

The equilibrium binding responses (association phase peaks) were fit via nonlinear regression to eq 5 using Kaliedagraph:

$$RRU = \frac{k_{assn}[TGT][RNA]}{K_D* + [RNA]} \quad (5)$$

where RRU is the relative response units and K_D* is the "thermodynamic" dissociation constant.

RESULTS

Steady-State Kinetics for ECYMH and (dG)$_{34}$-ECYMH. In previous studies, we observed that hairpin RNAs (~25 bases in length) corresponding to the anticodon stem−loop region of TGT substrate tRNAs are suitable substrates for *E. coli* TGT (*9*−*11*). We have also shown that within these substrates, the guanosine corresponding to tRNA position 34 can be replaced with a 2′-deoxyriboside without affecting steady-state kinetic values (*11*). The relative ease of synthesis and biotinylation of hairpin RNAs prompted their use in studying the kinetic details of the TGT reaction. The biotinylation of the substrate RNAs was necessary for the surface plasmon resonance experiments. Importantly, control experiments demonstrated that this chemical modification had no effect on the interaction of the RNA with TGT (data not shown). Steady-state kinetic parameters were determined for ECYMH and (dG)$_{34}$ECYMH by following the incorporation of [^{3}H]preQ$_1$ into the RNA substrate (Figure 4). The values were essentially identical with a slightly higher k_{cat} for (dG)$_{34}$ECYMH.

Rate of Covalent Intermediate Formation. We have reported using rapid-quench kinetics as a technique to characterize covalent enzyme−RNA intermediates (*8*). The apparent rates of formation of the covalent intermediates for ECYMH and

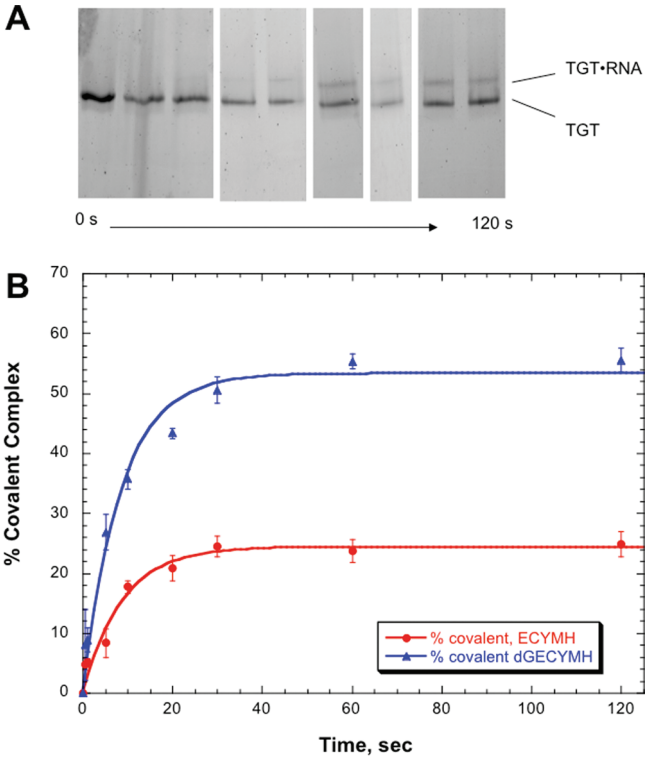

FIGURE 5: Kinetics of covalent complex formation for ECYMH and (dG$_{34}$)ECYMH. (A) SDS−PAGE of TGT and TGT−ECYMH covalent complex vs time. Samples were obtained via a rapid-quench method as described in Experimental Procedures. (B) Fit of % covalent vs time to an exponential binding equation: % covalent = $A[1 - \exp(-k_{formation}t)]$, where A is the maximum % covalent achieved. Error bars show the standard deviations of time points from triplicate runs.

Table 1: Apparent Rates[a] of Formation and Breakdown of the Covalent Intermediate

RNA	apparent $k_{formation}$ (s^{-1})	apparent $k_{breakdown}$ (s^{-1})	k_{cat} (s^{-1})
ECYMH	0.114 ± 0.021	nd[b]	0.0094 ± 0.0007
(dG$_{34}$)ECYMH	0.118 ± 0.017	0.50 ± 0.14	0.011 ± 0.0007

[a]Rates include the standard error of the fits. [b]Not determined.

(dG)$_{34}$ECYMH were determined with this technique (Figure 5 and Table 1). Again, the apparent rates of formation for both RNAs are essentially identical. In this experiment, guanine is released, either bound to the covalent enzyme−RNA complex or free in solution. Given that TGT can catalyze a guanine for guanine base-exchange reaction, it is possible that the displaced guanine can attack the covalent complex, re-forming noncovalently bound substrate RNA. This activity accounts for the equilibrium of covalent and noncovalent complexes that is observed in these experiments. Interestingly, the two RNAs achieve different equilibrium extents of covalent intermediate formation (Figure 5B), with ECYMH reaching ~25% and (dG)$_{34}$-ECYMH at ~55%.

Rate of Covalent Intermediate Breakdown. The rate of covalent intermediate breakdown proved to be much more difficult to study. To do so, the TGT−RNA covalent intermediate must first be formed and isolated. Once isolated, the breakdown of the intermediate can be evaluated using the same rapid-quench strategy employed in the formation studies. Unfortunately,

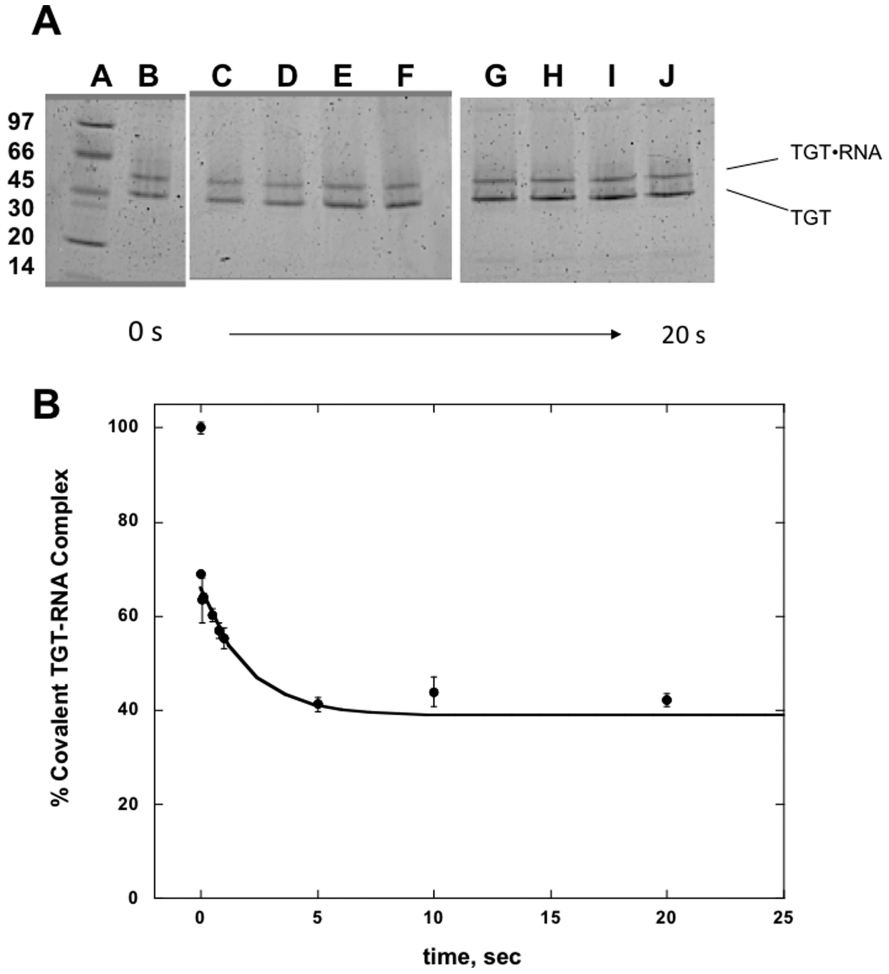

FIGURE 6: Kinetics of covalent complex breakdown for (dG_{34})ECYMH. (A) SDS−PAGE of TGT and the TGT−RNA covalent complex vs time. Samples were obtained via the rapid-quench technique as described in Experimental Procedures. (B) Fit of % covalent vs time to a single-exponential decay: % covalent $= (A - B) \times \exp(-k_{\text{formation}}t) + B$, where A is the initial % covalent (after the first rapid phase) and B is the limiting % covalent. Note that the first data point was omitted from the fit. See Results for a discussion. Error bars show the standard deviations of time points from four runs.

Table 2: Binding and Steady-State Kinetic Parameters[a]

RNA	k_{on} (M^{-1} s^{-1})	k_{off} (s^{-1})	K_D (μM) (k_{off}/k_{on})	K_D* (μM)	k_{cat} (s^{-1})	K_M (μM)
ECYMH	39000 ± 1000	0.013 ± 0.001	0.33 ± 0.11	0.21 ± 0.04	0.0094 ± 0.0007	2.87 ± 0.77
$(preQ_1)$ECYMH	17000 ± 9600	0.010 ± 0.005	0.66 ± 0.33	0.46 ± 0.05	na[b]	na[b]
(dG_{34})ECYMH	84000 ± 28000	0.026 ± 0.001	0.31 ± 0.11	0.35 ± 0.02	0.011 ± 0.0007	2.62 ± 0.62
$(dpreQ_1)$ECYMH	74000 ± 22000	0.021 ± 0.005	0.28 ± 0.16	0.61 ± 0.02	na[b]	na[b]

[a]On and off rate constants were determined from a fit to a two-state model (eq 4). Only the values for the on and off rate constants were used to calculate K_D values. The full set of values can be found in the Supporting Information. K_D* was determined from a "thermodynamic fit" of association peak values (Figure 7). K_M and k_{cat} values were determined from Michaelis−Menten fits (Figure 7). Parameters are reported with the standard error of the fits. [b]Not applicable as $(preQ_1)$ECYMH is not a substrate.

only the $(dG)_{34}$ECYMH−TGT covalent intermediate proved to be amenable to isolation, and even so, the isolated species consisted of a 1:1 mixture of unbound enzyme and covalent intermediate (Figure 6A). Analysis of the rapid-quench data suggests that the breakdown of this intermediate follows biphasic kinetics (Figure 6B). Interestingly, the first phase of the reaction was too rapid to obtain accurate data. Consequently, the first data point was omitted in the fitting of the second, slower phase. Because of the technical difficulties associated with these experiments, the apparent rate of breakdown for $(dG)_{34}$ECYMH (Table 2) should be viewed as an estimate only for the slower phase.

Association and Dissociation Kinetics. Surface plasmon resonance (SPR) was employed to determine the rates of association and dissociation of the RNA and TGT. Wild-type TGT will rapidly form a covalent complex with RNA bound to the sensor chip, complicating association and dissociation studies. Therefore, we elected to use a TGT mutant, TGT(D264N), which we have previously shown to be inactive and incapable of forming the covalent intermediate, while maintaining the ability to bind noncovalently to RNA (*5*, *6*). The biotinylated RNAs were bound to a streptavidin-coated sensor chip, and TGT-(D264N) was passed over the chip. Figure 2 of the Supporting Information shows an example of a sensorgram for one

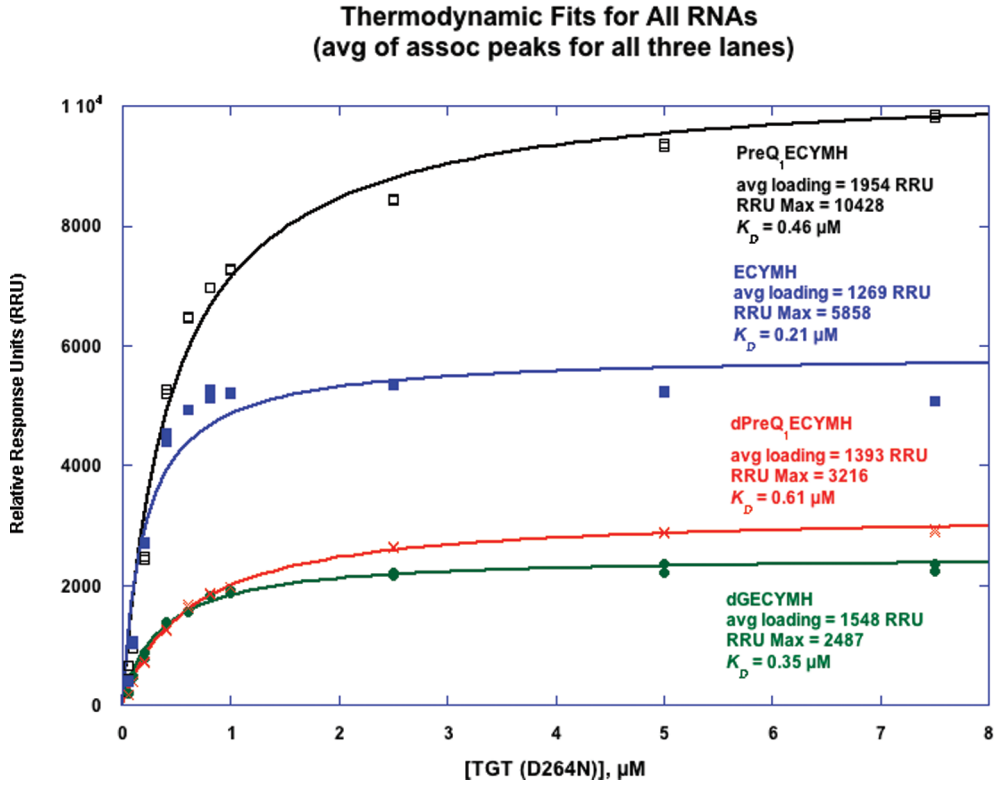

FIGURE 7: Thermodynamic fit of SPR association peak values to determine K_D* values. Association peak RU values of replicate runs for each RNA were fit to the steady-state binding equation: $RU_{obs} = \{RU_{max}[TGT(D264N)]\}/\{K_D + [TGT(D264N)]\}$. The average RNA loadings for each chip are indicated.

concentration of TGT(D264N) flowing over three RNA-bound lanes (different RNA loadings indicated) and one control lane on a single chip.

For each concentration of TGT(D264N), the association phase was followed to the point where equilibrium binding was established (e.g., the association peak). The average relative response unit values corresponding to the association peaks for the various TGT(D264N) concentrations were fit to determine thermodynamic K_D values for the RNAs (Figure 7 and Table 2). Different amounts of RNA were intentionally loaded in the three sample lanes on each sensorchip to control for loading-dependent artifacts (see Discussion). One would expect that the maximum amount of TGT(D264N) bound in each lane (e.g., RRU plateau values) would correlate with the amount of RNA loaded. This is in fact the case within each chip, as shown in Figure 3 of the Supporting Information (an example of the thermodynamic fits for each lane of a single chip). The trend in plateau values matches the trend in RNA loading for the lanes. This was observed for all RNAs examined in these studies (data not shown). Interestingly, from chip to chip (i.e., different RNAs), the plateau RRU values do not correlate with the average RNA loadings. Thus, it is likely that the absolute RRU values vary more from chip to chip than with the loading.

The association and dissociation phases were globally fit to a two-state ("conformational change") model (eq 4). (Figure 4 of the Supporting Information shows one example of the fitted association and dissociation curves.) The fit yielded values for the rate constants shown in eq 4. (Table 2 of the Supporting Information lists all of these values.) In Table 2, the values for k_{on}, k_{off}, and K_D calculated from these rate constants are reported. Fitting to a two-state model is not sufficient to prove the existence of a conformational change, as SPR is insensitive to conformational change (BIA Evaluation Software Manual). To date, independent evidence to support a conformational change in the TGT reaction is lacking. Furthermore, because of technical reasons discussed above, an inactive TGT mutant is employed in these SPR studies. It is possible that this mutant enzyme or the RNA substrate may exhibit a conformational change that would not be present in the wild-type TGT reaction where the binding of the heterocyclic substrate would drive the reaction forward. Given these issues, the conformational change is somewhat underdefined; therefore, we choose to define K_D as the equilibrium constant for the initial binding of RNA and exclude the putative subsequent conformational change. As shown in Table 2, the K_D values calculated from the association and dissociation rate constants match very well with the thermodynamic K_D* values determined from the association peak fits, consistent with the discussion given above.

DISCUSSION

Previously published data from our laboratory strongly support an associative molecular mechanism for the TGT reaction (*5*, *7*). The X-ray crystal structure of the TGT from *Z. mobilis*, determined in the presence of the RNA substrate, offers further evidence for this hypothesis (Figure 3) (*12*). Specifically, this structure unequivocally demonstrates that TGT is capable of forming a covalent linkage with RNA. Together, these biochemical and structural studies implicate the formation of a covalent intermediate during TGT catalysis.

However, proof of the existence of an intermediate on a reaction pathway requires three generally accepted criteria (*13*). First, the intermediate should be isolable. Second, the reaction intermediate should be chemically competent (i.e., forms from

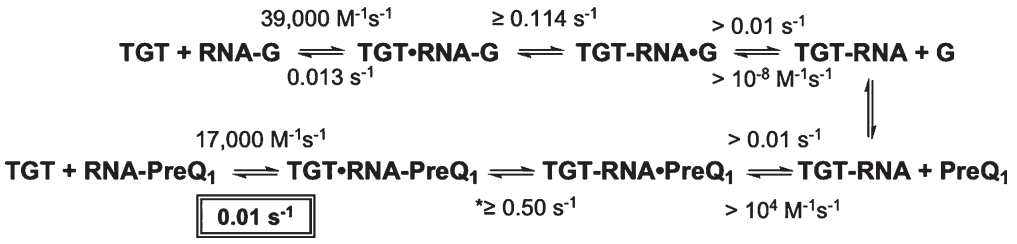

FIGURE 8: *E. coli* TGT kinetic mechanism with rate constant values. The rate constant for the chemical step of formation of the covalent intermediate is a lower limit estimated from $k_{formation}$. The rate constant for the breakdown of the covalent intermediate (*0.50 s^{-1}) is an estimate of the slower phase. Lower limits for the on and off rates for guanine and $preQ_1$ can be made by setting the lower limit for the forward steps (off rate for guanine and on rate for $preQ_1$) greater than or equal to 0.01 s^{-1} (k_{cat}). Assuming K_M approximates K_D, then lower limits for the other rates can be set by simple division ($K_D = k_{off}/k_{on}$). The overall rate-determining step is the dissociation of product tRNA (boxed).

substrates and can turn over to the correct products). Finally, the reaction intermediate should be kinetically competent (i.e., can form and react at a rate that is greater than or equal to k_{cat}). The elucidation of the TGT−RNA cocrystal structure has indeed demonstrated that a TGT−RNA covalent intermediate is isolable. Furthermore, upon soaking the crystals with $preQ_1$, Xie et al. observed turnover of the TGT−RNA intermediate which generated free enzyme (*12*). This observation is in strong agreement with work from our laboratory in which it was observed that the TGT−RNA covalent complex could be converted to free TGT in solution upon the addition of $preQ_1$. Together, these independent observations indicate that the TGT−RNA covalent intermediate is chemically competent.

Previously, Geeganage and Frey (*14*) employed a rapid-quench approach to determine the kinetic competence of a uridyl−enzyme intermediate in the galactose-1-phosphate uridylyltransferase reaction in which the formation of the uridyl−enzyme intermediate was followed upon mixing a single concentration of enzyme with saturating substrate under single-turnover conditions (see Figure 3 of their paper). Comparison of the resulting first-order rate constant (281 s^{-1}) with k_{cat} (62 s^{-1}) led to the authors' conclusion that the formation of the covalent intermediate is kinetically competent. To establish the kinetic competence of the putative TGT−RNA covalent intermediate, we conducted a similar study in an effort to determine the apparent first-order rate constant of intermediate formation for wild-type TGT. In the case of the TGT reaction, this observed rate constant ($k_{formation}$) is a combination of at least four individual rate constants, as shown in Figure 2. Additional information is required to deconvolute $k_{formation}$ to obtain the microscopic rate constant for the chemical step of intermediate formation. The observed formation rate constants for ECYMH and $(dG)_{34}$ECYMH are essentially identical [ca. 0.12 s^{-1} (Table 1)] and 10-fold faster than k_{cat} (0.01 s^{-1}) (Table 2), thereby demonstrating that formation of the covalent intermediate is fast enough to be on the TGT reaction pathway. Moreover, given that k_{cat} is representative of the rate-limiting step, this comparison indicates that formation of the covalent intermediate is not rate-limiting in the TGT reaction.

The breakdown of the TGT−RNA covalent complex was also interrogated using the same rapid-quench approach. Unfortunately, the TGT−ECYMH covalent complex could not be isolated in sufficient quantities for characterization. However, the covalent complex with $(dG)_{34}$ECYMH was amenable to isolation and follow-up study. The breakdown of this covalent complex exhibited biphasic breakdown kinetics (Figure 6). The slower phase was determined to be 0.50 s^{-1}, which, like the rate of formation ($k_{formation}$), is much faster than k_{cat}. These studies were conducted under pseudo-first-order conditions (e.g., saturating $preQ_1$), eliminating the $preQ_1$ binding step in the kinetics. Therefore, this observed breakdown rate can be viewed as a lower limit for the true chemical breakdown step as any back reaction, re-forming the covalent intermediate prior to product release, would reduce the observed rate. This proves that even the slower phase of covalent complex breakdown is also fast enough to be on the TGT reaction pathway and is not the rate-limiting step for the reaction. It should be noted that this experimental procedure involves denaturation of the enzyme−RNA complex; therefore, the loss of covalently bound complex is being monitored, regardless of whether the RNA is still noncovalently bound (i.e., RNA dissociation is not a factor).

The results from this work demonstrate that the covalent TGT−RNA complex is kinetically capable of existing on the TGT reaction pathway (i.e, kinetically competent). Moreover, because the rate constants measured in these studies are both faster than k_{cat}, neither chemical step (formation nor breakdown) nor binding of substrate RNA (part of the apparent rate of formation) can be rate-limiting in the TGT reaction. Thus, the identity of the rate-limiting step was still unknown.

Surface plasmon resonance, whereby biotinylated RNAs were bound to streptavidin-coated sensor chips, was employed to identify the rate-limiting step in the TGT reaction. It was immediately apparent that wild-type TGT could not be utilized in these experiments because of its propensity to bind the RNA and quickly form the covalent complex. This would preclude our ability to study the dissociation of the TGT−RNA noncovalent complex. To overcome this issue, an inactive TGT mutant [TGT(D264N)] in which the nucleophilic aspartate (264) is mutated to asparagine was employed in our SPR experiments. It has previously been demonstrated that this TGT mutant binds substrate RNA but is catalytically inactive and cannot form the covalent intermediate (*6*). Using this mutant, the association and dissociation rate constants, as well as the corresponding equilibrium dissociation constants for substrate [ECYMH and $(dG)_{34}$ECYMH] and product [$(preQ_1)_{34}$ECYMH and $(dpreQ_1)_{34}$ECYMH] RNAs, were determined (Table 2 and the Supporting Information). The experiments were conducted with three different loading levels of RNA on each chip relative to a control lane that contained no RNA. Similar kinetic values were obtained for all three RNA loading levels, eliminating the possibility of any "rebinding" or other loading-dependent artifacts in the SPR experiments. Within each chip, the maximum RRU values for each lane correlated with the RNA loading (Figure 3 of the Supporting Information), as would be expected. Thermodynamic fits of the association phase peak values versus the enzyme concentration yielded K_D values that correlated well

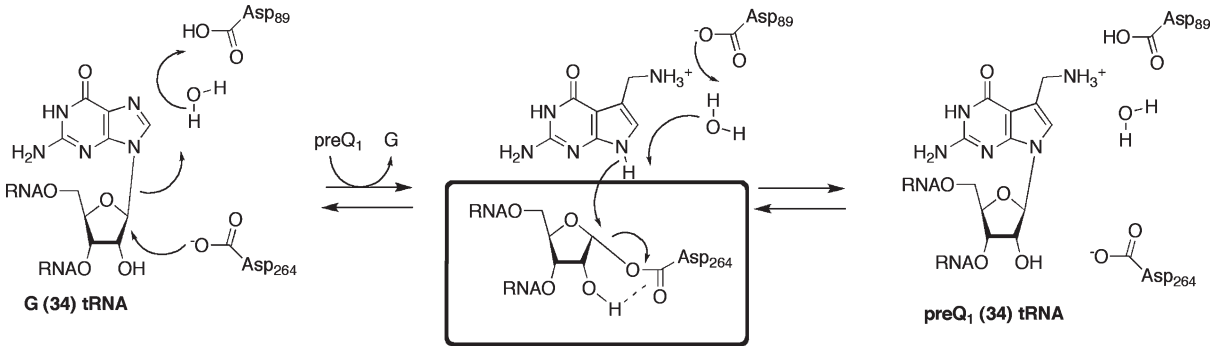

FIGURE 9: Proposed role of the 2′-hydroxyl group in the breakdown of the TGT−RNA covalent complex.

with those from the kinetic fits (Table 2). These controls establish the validity of the SPR kinetic determinations.

The resulting sensorgrams were globally fit using BIA Evalution. The association rate constants were all very high (Table 2). For example, at saturation (e.g., 20 μM RNA), the association rate for ECYMH would be $\sim$0.8 s^{-1}, roughly 80-fold faster than k_{cat}. This fast association rate is consistent with the apparent rate of formation ($\sim$0.1 s^{-1}) that was measured in the rapid-quench studies, suggesting that the observed rate of formation can be attributed to the chemical step. In contrast, the dissociation rate constants (Table 2) are much slower and comparable to k_{cat} [e.g., (preQ$_1$)ECYMH dissociation rate of 0.010 s^{-1}, k_{cat} of 0.0094 s^{-1}]. As mentioned above, the kinetically determined K_D values correlate very well with those from the thermodynamic fits (Table 2).

Figure 8 shows the kinetic mechanism for TGT with the rate constants that have been determined in these studies. Lower limits for the dissociation of guanine ($>$0.01 s^{-1}) and the association of preQ$_1$ ($>10^4$ M^{-1} s^{-1}) can be set given that they cannot be lower than k_{cat} [i.e., at $\sim10^{-6}$ M preQ$_1$ ($\sim K_M$), one would observe an on rate of 0.01 s^{-1}]. By assuming that the K_M values for both guanine and preQ$_1$ approximate K_D values and are in the micromolar range, lower limits for the association of guanine ($>10^4$ M^{-1} s^{-1}, same estimation as for preQ$_1$) and the dissociation of preQ$_1$ ($>$0.01 s^{-1}) can be set by simple division ($K_D = k_{off}/k_{on}$). Our SPR experiments indicate that the binding of RNA (substrate and product) to TGT is much faster than the apparent $k_{formation}$ that we have measured from single-turnover, rapid-quench studies. Therefore, it is reasonable to assign $k_{formation}$ as a lower limit for the chemical formation rate; any reverse reaction would mean that the chemical step would be faster than $k_{formation}$. While we were only able to estimate the observed breakdown rate for the slower phase for $(dG)_{34}$-ECYMH, given the pseudo-first-order conditions, this value is a reasonable lower limit for the chemical breakdown step. From this, it is apparent that the dissociation of the product RNA is the overall rate-limiting step in the reaction.

It has previously been shown that the 2′-hydroxyl group of G34 is not requisite for the TGT reaction (*11*). Both the rates of formation and k_{cat} values for the RNA and 2′-deoxy RNA are essentially identical (Table 2). However, only the $(dG)_{34}$ECYMH covalent intermediate was isolated sufficiently to enable the measurement of the rate of breakdown. Presumably, the ECYMH covalent complex is significantly less stable (i.e., the equilibrium between the covalent complex and bound/free guanine and noncovalently bound RNA lies more toward the noncovalent complex). This is consistent with observations noted in the formation rapid-quench studies in which, for ECYMH, the maximum extent of covalent complex formed was approximately half of that for $(dG)_{34}$ECYMH. This suggests that the rate of the back reaction for ECYMH (similar to breakdown but with guanine instead of preQ$_1$) is twice that for $(dG)_{34}$ECYMH. The 2′-hydroxyl group of G34 is located in a position to stabilize the incipient charge on aspartate 264 in the transition state for covalent complex breakdown (or the reverse of formation), as schematically depicted in Figure 9. Additionally, a strong hydrogen bond could be formed between the 2′-hydroxyl group of G34 and the charged aspartate 264 in the ground-state complex (perhaps mediated by a water molecule). In either event, the result would be stabilization of either the transition state or the ground state relative to that for $(dG)_{34}$ECYMH, resulting in faster collapse of the intermediate for ECYMH.

In summary, these studies have unequivocally demonstrated that the TGT−RNA covalent complex is kinetically competent to be on the TGT reaction pathway. The evaluation of the rate constants for various chemical and binding steps has revealed that the dissociation of product RNA from the enzyme is overall rate-limiting in the steady state. Further, studies comparing RNA with a 2′-deoxyriboside at the site of modification suggest a role for the 2′-hydroxyl group in stabilizing the growing negative charge on the nucleophilic aspartate (264) as the glycosidic bond to the aspartate is broken during covalent complex breakdown.

ACKNOWLEDGMENT

We thank Prof. Carol Fierke and Dr. Katherine Bowers for assistance with the rapid-quench experiments and Prof. Jason Gestwicki and Mr. Srikanth Patury for assistance with the BIAcore SPR studies and helpful discussions. We also acknowledge the assistance of James Windak in the mass spectrometry facility of the Department of Chemistry, University of Michigan.

SUPPORTING INFORMATION AVAILABLE

MALDI-TOF mass spectrometry analyses of hairpin RNAs, table of two-state fit parameters, TGT active site sequence alignments showing conservation of aspartates, example of a thermodynamic fit of SPR association peak values for three lanes of a single sensor chip, and an example of a complete set of fitted sensorgrams for a single lane (i.e., one trial for a single RNA). This material is available free of charge via the Internet at http://pubs.acs.org.

REFERENCES

1. Grosjean, H., and Benne, R. (1998) Modification and Editing of RNA: The Alteration of RNA Structure and Function, ASM Press, Washington, DC.

2. Spedaliere, C. J., et al. (2004) The pseudouridine synthases: Revisiting a mechanism that seemed settled. *J. Am. Chem. Soc. 126*, 12758–12759.
3. Romier, C., et al. (1996) Mutagenesis and crystallographic studies of *Zymomonas mobilis* tRNA-guanine transglycosylase reveal aspartate 102 as the active site nucleophile. *Biochemistry 35*, 15734–15739.
4. Zechel, D. L., and Withers, S. G. (2000) Glycosidase mechanisms: Anatomy of a finely tuned catalyst. *Acc. Chem. Res. 33*, 11–18.
5. Kittendorf, J. D., et al. (2001) tRNA-guanine transglycosylase from *Escherichia coli*: Molecular mechanism and role of aspartate 89. *Biochemistry 40*, 14123–14133.
6. Kittendorf, J. D., et al. (2003) An essential role for aspartate 264 in catalysis by tRNA-guanine transglycosylase from *Escherichia coli*. *J. Biol. Chem. 278*, 42369–42376.
7. Goodenough-Lashua, D. M., and Garcia, G. A. (2003) tRNA-Guanine Transglycosylase from *Escherichia coli*: A Ping-Pong Kinetic Mechanism is Consistent with Nucleophilic Catalysis. *Bioorg. Chem. 31*, 331–344.
8. Chervin, S. M., Kittendorf, J. D., and Garcia, G. A. (2007) Probing the Intermediacy of Covalent RNA-Enzyme Complexes in RNA Modification Enzymes. *Methods Enzymol. 425*, 121–137.
9. Curnow, A. W., et al. (1993) tRNA-Guanine Transglycosylase from *Escherichia coli*: Gross tRNA Structural Requirements for Recognition. *Biochemistry 32*, 5239–5246.
10. Nonekowski, S. T., and Garcia, G. A. (2001) tRNA Recognition by the *E. coli* TGT: The Role of U33 in U-G-U Sequence Recognition. *RNA 7*, 1432–1441.
11. Nonekowski, S. T., Kung, F. L., and Garcia, G. A. (2002) The *Escherichia coli* tRNA-Guanine Transglycosylase Can Recognize and Modify DNA. *J. Biol. Chem. 277*, 7178–7182.
12. Xie, W., Liu, X. J., and Huang, R. H. (2003) Chemical trapping and crystal structure of a catalytic tRNA guanine transglycosylase covalent intermediate. *Nat. Struct. Biol. 10*, 781–788.
13. Fersht, A. (1999) Structure and Mechanism. In Protein Science: A Guide to Enzyme Catalysis and Protein Folding, W. H. Freeman and Company, New York.
14. Geeganage, S., and Frey, P. A. (1998) Transient Kinetics of Formation and Reaction of the Uridylyl-Enzyme Form of Galactose-1-P Uridylyltransferase and Its Q168R Variant: Insight into the Molecular Basis of Galactosemia. *Biochemsitry 37*, 14500–14507.